OS-4-002

Fifth International Symposium on Cavitation (cav2003)
Osaka, Japan, November 1-4, 2003

ROTORDYNAMIC FLUID FORCES ON WHIRLING AND CAVITATING RADIAL IMPELLERS

Luca d'Agostino
Professor, Dipartimento di Ingegneria Aerospaziale, Università di Pisa, Via G. Caruso, 56126 Pisa, Italy
luca.dagostino@ing.unipi.it

Marco R. Venturini Autieri
M.S. Student, Dipartimento di Ingegneria Aerospaziale, Università di Pisa, Via G. Caruso, 56126 Pisa, Italy
turbopump@libero.it

ABSTRACT

This paper investigates the linearized dynamics of the rotordynamic forces exerted by the fluid on the rotor in whirling and cavitating radial impellers with thin logarithmic blades and constant eccentricity and whirl speed. The flow is modeled as an incompressible, inviscid, fully-guided liquid except on the suction sides of the blades, where attached cavitation occurs in a small layer of given acoustic admittance depending on the assumed values of the layer thickness and void fraction. Constant boundary conditions for the total pressure are imposed at the inlet and outlet sections. The three-dimensional unsteady governing equations are written in rotating orthonormal logarithmic spiral coordinates, linearized for small-amplitude whirl perturbations of the mean steady flow, and solved by modal decomposition. Rotordynamic fluid forces in centrifugal pumps are found to be almost insensitive to cavitation; also, they do not undergo the internal flow resonances in the blade channels predicted by similar flow models and observed in whirling and cavitating axial inducers. Comparison with the available experimental results shows that the present theory underestimates the intensity of rotordynamic impeller forces, but correctly captures their observed parabolic trend as functions of the whirl frequency, thus indicating that it can usefully contribute to identify the main physical phenomena involved and provide useful practical indications on their dependence on the relevant flow conditions and parameters.

INTRODUCTION

Local flow phenomena like tip leakage capable of interfering with the fluid dynamic loads on the blades are known to be the dominant source of rotordynamic whirl forces in compressible flow machines (Thomas, 1958 [1], Alford, 1958 [2], Martinez-Sanchez et al., 1995 [3], Song and Martinez-Sanchez, 1997a [4], Martinez-Sanchez, 1997b [5]). On the other hand, in turbopumps also the reaction of the entire flow to the impeller whirl motion can often be significant (d'Auria, d'Agostino and Brennen, 1995 [6]; d'Agostino and d'Auria, 1997 [7]; d'Agostino, d'Auria and Brennen, 1998 [8], d'Agostino and Venturini, 2002 [9]). Previous turbopump research has mainly focused on the origin and analysis of rotordynamic impeller forces in noncavitating conditions (Chamieh et al., 1985 [10]; Jery, Acosta and Caughey, 1985 [11]; Jery, 1987 [12]; Shoji and Ohashi, 1987 [13]; Ohashi and Shoji, 1987 [14]; Adkins and Brennen, 1988 [15]; Arndt et al., 1989 [16]; Arndt et al., 1990 [17]; Tsujimoto et al., 1997 [18]; Uy and Brennen, 1999 [19]; Baskharone, 1999 [20], Hiwata and Tsujimoto, 2002 [21]).

Because of their greater complexity, rotordynamic fluid forces in whirling and cavitating turbopump impellers have so far received comparatively less attention in the open literature and a satisfactory understanding of their behavior is still lacking. However, it is widely recognized that turbopump cavitation in axial inducers can promote the onset of dangerous self-sustained whirl instabilities (Rosenmann, 1965 [22]) and substantially alters the behavior of fluid-induced rotordynamic forces (Arndt and Franz, 1986 [23]; Brennen, 1994 [24]; Bhattacharyya, 1994 [25]). The available experimental evidence indicates that inducer cavitation reduces the magnitude of the rotordynamic fluid forces, significantly affecting the added mass of the rotor. The consequent increase of the critical speeds is of special relevance to highly-loaded supercritical machines, as commonly used in liquid propellant rocket feed systems. A second major effect of inducer cavitation is the introduction of a complex oscillatory dependence of the rotordynamic fluid forces on the whirl frequency. This finding seems to indicate the occurrence of resonance phenomena in the compressible cavitating flow inside the blade channels under the excitation imposed by the eccentric motion of the rotor. Earlier theoretical analyses confirmed the presence of internal flow resonances and indicate that bubble dynamic effects do not play a major role, except, perhaps, at extremely high whirl speeds (d'Auria, d'Agostino and Brennen, 1995 [26]; d'Agostino and d'Auria, 1997 [27]; d'Agostino, d'Auria and Brennen, 1998 [28], d'Agostino and Venturini, 2002 [9]). On the other hand, no resonant phenomena seem to occur radial impellers, where the limited available evidence indicates that cavitation only has a marginal effect on rotordynamic whirl forces (Franz et al., 1989 [29]). Following up on our work on whirling and cavitating inducers, we now apply a similar approach to the analysis of the unsteady two-dimensional flow in whirling radial impellers with

attached blade cavitation, in order to gain some better understanding of the fundamental reasons for the different behavior of rotordynamic fluid forces in this kind of machines. Upon introduction of suitable simplifying approximations, the flow is linearized for small-amplitude whirl motions of the rotor and solved by modal expansion. In spite of the simplifications introduced in order to obtain an efficient closed form solution, comparison with the available experimental data shows that the present analysis correctly predicts some of the observed features of the rotordynamic fluid forces in cavitating inducers and provides useful practical indications of their dependence on the relevant flow conditions and parameters.

NOMENCLATURE

a	sound speed
b	axial length of the inducer
c	constant
$\boldsymbol{e}$	unit vector
E	cavitation parameter
F	force
i	imaginary unit
j	blade index
K_E	cavitating layer parameter
m	streamwise mode index
n	blade-to-blade spiral coordinate
N_B	number of blades
O, O^*	origins of coordinate systems
p	pressure
p_t	total or stagnation pressure
r	radial coordinate, radius
$\boldsymbol{r}$	radial vector
s	streamwise spiral coordinate
t	time
T	aspect ratio
$\boldsymbol{u}$	velocity vector
v	azimuthal velocity component
z	axial coordinate
α	void fraction
β	blade angle
δ	cavitation layer thickness
ε	whirl eccentricity
ϑ	azimuthal angle
ρ	density
φ	velocity potential
ω	whirl angular speed
Ω	impeller rotational speed

Subscripts and superscripts

C	cavitation
F	mean flow
H	hub
L	liquid
R	radial
T	tangential, blade tip
$\overline{q}$	unperturbed value of q
$\tilde{q}$	perturbation value of q
$\hat{q}$	complex representation of q
q'	derivative, value of q in the rotating frame
q^*	value of q in the inducer-fixed frame

LINEARIZED DYNAMICS OF THE CAVITATING FLOW IN A WHIRLING INDUCER

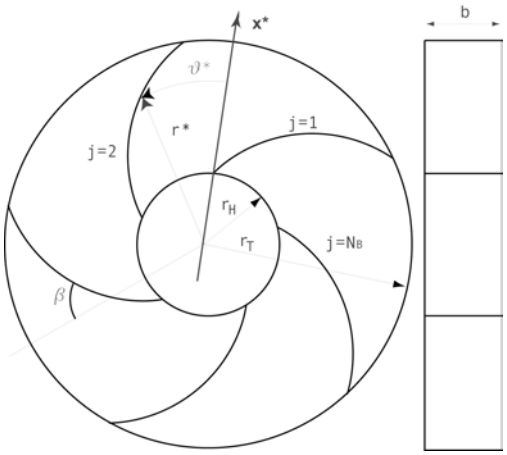

Figure 1. Schematic of the pump geometry

We examine the dynamics of an incompressible, inviscid liquid of velocity $\boldsymbol{u}$, pressure p, and density ρ_L in a centrifugal pump rotating with velocity Ω and whirling on a circular orbit of small eccentricity ε at angular speed ω. A number of idealizations are introduced in order to obtain an analytical solution. Figure 1 illustrates the simple centrifugal pump considered, with N_B logarithmic-spiral blades of equation $rd\vartheta/r = -\tan\beta$, zero blade thickness, axial length b, hub radius r_H, tip radius r_T, blade angle β.

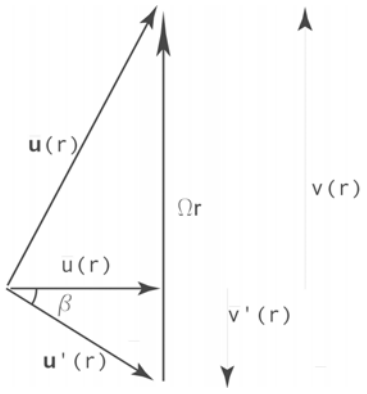

Figure 2. Velocity triangle.

The flow is fully wetted everywhere except on the suction sides of the blades, where attached cavitation occurs. The mean flow velocity $\overline{\boldsymbol{u}}$ in the blade channels (Fig. 2) is specified by the flow coefficient $\phi = \overline{u}_T / \Omega r_T$, assuming fully-guided forced-vortex flow with zero axial velocity $\overline{w}$, radial velocity $\overline{u} = r_T \overline{u}_T / r$, and tangential velocity:

$$\overline{v}^2 = \Omega^2 \phi^2 \left(r_T^4 / r^2 \right) \tan^2\beta + \Omega^2 r^2 - 2\Omega^2 r_T^2 \phi \tan\beta$$

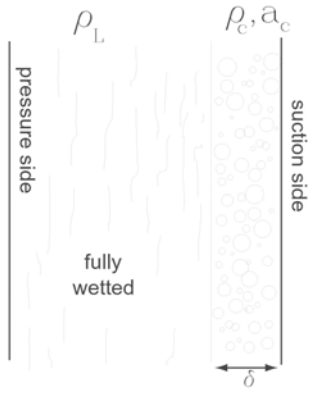

Figure 3. Cavitating layer.

With reference to Figure 3, cavitation is thought to occur on the suction sides of the blades in a thin layer of given variable thickness δ (constant coordinate n, see below) and acoustic admittance $\rho_C a_C^2$. For simplicity, it is also assumed that the static pressure p_C in the cavitating layer is nearly equal to the total pressure p_t of the surrounding liquid.

We define stationary cylindrical coordinates r,ϑ,z with center in O on the axis of the stator, rotating cylindrical coordinates r',ϑ',z' spinning at the rotor speed with center in the same point O, and rotating and whirling cylindrical coordinates r^*,ϑ^*,z^* fixed in the inducer and with center in O^* on its geometric axis. Then the equations of the blade surfaces are:

$$b = \ln\frac{r}{r_H} + (\vartheta - \vartheta_j)\cot\beta = 0$$

where $\vartheta_j = 2\pi(j-1)/N_B$ is the angular location of the j-th blade for $j = 1,2,...,N_B$. The flow velocities in the stationary and rotating frames are related by $\boldsymbol{u} = \boldsymbol{u}' + \boldsymbol{\Omega}\times\boldsymbol{r}$ and, to the first order in the eccentricity (Fig. 4):

$$r^* = r - \varepsilon\cos(\vartheta - \omega t) = r' - \varepsilon\cos(\vartheta' - \omega' t)$$

$$\vartheta^* = \vartheta - \Omega t + \frac{\varepsilon}{r}\sin(\vartheta - \omega t) = \vartheta' + \frac{\varepsilon}{r}\sin(\vartheta' - \omega' t)$$

$$z^* = z' = z\,.$$

where $\omega' = \omega - \Omega$.

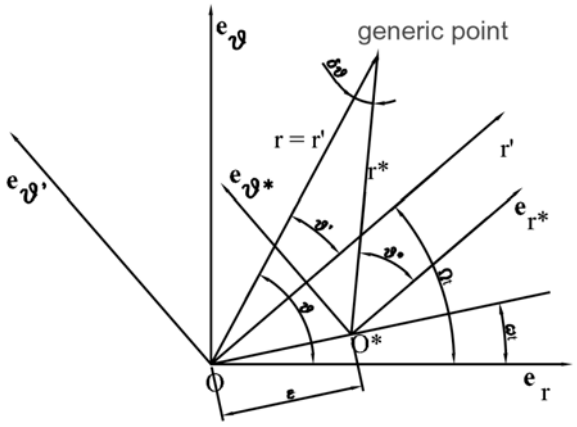

Figure 4. Schematic of whirl motion and coordinates.

The perturbation velocity $\tilde{\boldsymbol{u}}$ generated by the blade motion is irrotational ($\tilde{\boldsymbol{u}} = \nabla\varphi$) because the flow originates from a uniform stream. Therefore, in the rotating frame the flow velocity is $\boldsymbol{u}' = \boldsymbol{u} - \boldsymbol{\Omega}\times\boldsymbol{r}$ and the Bernoulli's equation writes:

$$\int\frac{\partial'\boldsymbol{u}'}{\partial t}\cdot d\boldsymbol{x} + \frac{1}{2}\boldsymbol{u}'\cdot\boldsymbol{u}' - \frac{1}{2}\Omega^2\boldsymbol{r}\cdot\boldsymbol{r} + \frac{p}{\rho_L} = B(t)$$

where $B(t)$ is the unsteady Bernoulli's constant. Hence the linearized governing equations for the flow perturbations (tildes) at any given point in the rotating frame are:

$$\nabla^2\tilde{\varphi} = 0 \qquad \text{and} \qquad \frac{\partial'\tilde{\varphi}}{\partial t} + \overline{\boldsymbol{u}}'\cdot\nabla\tilde{\varphi} + \frac{\tilde{p}}{\rho_L} = 0$$

Here the flow velocity must satisfy the kinematic conditions $Db/Dt = 0$ on the hub, blade and casing surfaces of equations $b = 0$ in the relevant coordinates. In addition, the total pressure is assumed constant on the inlet and outlet sections of the inducer.

In order to simplify the derivation of the solution, let us introduce orthogonal spiral coordinates n,s (Campos and Gil, 1995 [30]; Visser, 1999 [31]) as shown in Figure 5, with:

$$n = \frac{N_B}{2\pi}(\vartheta - \vartheta_j) + \frac{N_B}{2\pi}\ln\left(\frac{r}{r_H}\right)\tan\beta$$

$$n = -\frac{\sin\beta\cos\beta}{\ln(r_T/r_H)}(\vartheta - \vartheta_j) + \frac{\ln(r/r_H)}{\ln(r_T/r_H)}\cos^2\beta$$

For convenience, n and s are normalized to map a channel into a rectangle $(0,1)\times(0,1)$. Rotating and body-fixed orthogonal spiral coordinates n',s' and n^*,s^* are similarly defined in terms of r',ϑ' and r^*,ϑ^*. The third dimension z is easily added. Then, the equations of the inlet, blade pressure side, blade suction side and outlet surfaces are:

$$b = s^* = 0\,.$$
$$b = n^* = 0\,.$$
$$b = n^* - 1 + \delta = 0\,.$$
$$b = s^* - 1 = 0\,.$$

where $\delta = \delta(t)$.

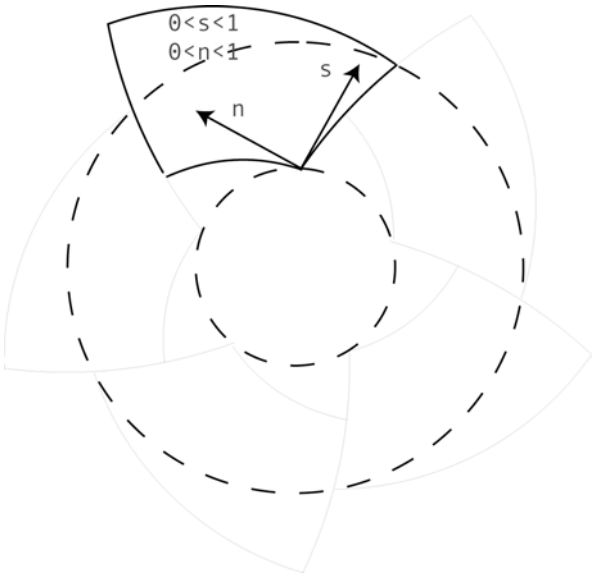

Figure 5. Schematic of the logarithmic-spiral coordinates.

From the continuity equation for the layer $\rho_C\delta \equiv \text{constant}$, the definition of $a_C^2 = dp/d\rho_C$ and the Bernoulli's equation $\tilde{p}/\rho_L \cong -\partial\tilde{\varphi}/\partial t$ it follows that:

$$\frac{d\delta}{dt} = \frac{\rho_L \delta}{\rho_C a_C^2}\frac{\partial^2\tilde{\varphi}}{\partial t^2}$$

With these results, and expressing $\nabla^2\tilde{\varphi} = 0$ and $\partial b/\partial t + \overline{\boldsymbol{u}}' \cdot \nabla b = 0$ in the rotating helical coordinates r', n', s':

$$\nabla'^2\tilde{\varphi} = \frac{\cos^2\beta}{\ln^2(r_T/r_H)}\frac{\partial^2\tilde{\varphi}}{\partial s'^2} + \frac{N_B^2}{4\pi^2\cos^2\beta}\frac{\partial^2\tilde{\varphi}}{\partial n'^2} = 0$$

and the linearized boundary conditions are found to be:

$$\frac{\partial\tilde{\varphi}}{\partial t} = 0 \qquad \text{on} \qquad s' = 1 \quad \text{and} \quad s' = 0$$

$$\frac{\partial\tilde{\varphi}}{\partial n'} = \varepsilon\frac{2\pi}{N_B}\left[\omega' r_H\left(\frac{r_T}{r_H}\right)^{s'}\cos^2\beta\sin\beta\left(\frac{\cos\Theta'}{\sin\beta}+\frac{\sin\Theta'}{\cos\beta}\right)+\right.$$

$$\left.+\left(\frac{r_T}{r_H}\right)^{1-s'}\overline{u}_T\sin\Theta'\right] \qquad \text{on} \qquad n' = 0$$

$$\frac{N_B}{2\pi}K_E\frac{\partial^2\tilde{\varphi}}{\partial t^2} + \frac{N_B}{2\pi r_H^2(r_T/r_H)^{2s'}\cos^2\beta}\exp\left(-\frac{4\pi}{N_B}\sin\beta\cos\beta\right)\frac{\partial\tilde{\varphi}}{\partial n'} =$$

$$= \varepsilon\omega'\frac{\sin\beta}{r_H(r_T/r_H)^{s'}}\exp\left(-\frac{2\pi}{N_B}\sin\beta\cos\beta\right)\left(\frac{\cos\Theta'}{\sin\beta}+\frac{\sin\Theta'}{\cos\beta}\right)+$$

$$+\varepsilon\frac{\overline{u}_T}{r_H^2}\left(\frac{r_T}{r_H}\right)^{1-3s'}\exp\left(-\frac{6\pi}{N_B}\sin\beta\cos\beta\right)\frac{\sin\Theta'}{\cos^2\beta} \qquad \text{on} \quad n' = 1$$

Here:

$$\Theta' = \vartheta' - \omega' t = \vartheta_j + \frac{2\pi}{N_B}n'\cos^2\beta - s'\ln\left(\frac{r_T}{r_H}\right)\tan\beta - \omega' t$$

and:

$$K_E = \frac{4\pi^2\rho_L\delta}{N_B^2\rho_C a_C^2}\cos^2\beta$$

is a parameter describing the dynamic behavior of the cavitating layer and the extent of cavitation.

With the above boundary conditions the Laplace equation for $\tilde{\varphi} = \mathrm{Re}\{\hat{\varphi}\}$ yields a well-posed boundary value problem for the complex velocity potential $\hat{\varphi}$. The separable solution in the blade channels is:

$$\hat{\varphi} = \sum_{m=1}^{+\infty}\left\{\left[c_1\cosh\left(n'\sqrt{\nu_m^2}\right)+c_2\sinh\left(n'\sqrt{\nu_m^2}\right)\right]\sin(m\pi s')\right\}e^{-i\omega' t}$$

with eigenvalues:

$$\sqrt{\nu_m^2} = i\frac{2m\pi^2\cos^2\beta}{N_B\ln(r_T/r_H)}$$

The instantaneous fluid force on the inducer is then:

$$\tilde{\boldsymbol{F}} = \int_{\text{blades}}\tilde{p}\left(\boldsymbol{r}'|_{\varepsilon\neq 0}, t\right)d\boldsymbol{S}$$

where, with second order error in the perturbations, the pressure:

$$\tilde{p} = -\rho_L\frac{\partial\tilde{\varphi}}{\partial t} - \rho_L\overline{\boldsymbol{u}}'\cdot\nabla\tilde{\varphi}$$

is evaluated for at the unperturbed position of the impeller ($\varepsilon = 0$). Because no hub is present, no buoyancy force acts on the displaced inducer due to the radial gradient of the mean pressure. The components of the instantaneous rotordynamic force are therefore obtained by integrating the projections of the elementary pressure forces along the axes of the whirling frame of center in O^* and unit vectors $\boldsymbol{e}_R, \boldsymbol{e}_T$, oriented as the eccentricity and its normal in the direction of the whirl motion. Finally, further integration over a period $2\pi/\omega'$ yields the time-averaged rotordynamic force $\boldsymbol{F}$ on the inducer.

The flow has then been determined in terms of the material properties of the two phases, the geometry of the inducer, the nature of the excitation, and the assigned quantities ϕ, δ, ρ_C, a_C.

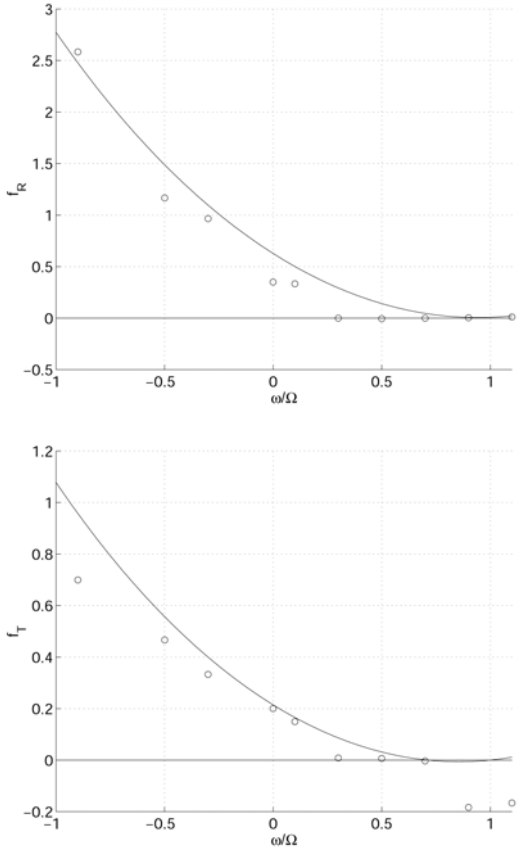

Figure 6. Comparison of the normalized radial and tangential rotordynamic forces, f_R and f_T, obtained from the present theory (continuous line) and the experimental results of Jery, 1987 [12] (divided by six, circles) for a centrifugal impeller with $\Omega = 1000$ rpm, $N_B = 5$, $\phi = 0.060$, $\beta = 23°$, $r_T = 81$ mm, $b = 16$ mm, $r_H/r_T = 0.5$ and $\Omega^2 K_E = 2$.

RESULTS AND DISCUSSION

In centrifugal pumps, the measured rotordynamic fluid forces in presence of cavitation are very similar to those for fully-wetted flows, consistently with the experimental results (Jery 1987 [12]; Franz et al., 1989 [29]). Therefore the rotordynamic fluid forces predicted by the present model are compared with the data measured by Jery, 1987 [12], at Caltech

on a five-bladed centrifugal pump with $r_T = 81$ mm, $r_H = 40$ mm, $\beta = 23°$, $b = 16$ mm, $\varepsilon = 0.126$ mm, without cavitation. The results obtained by Franz, 1989 [29], for a cavitating radial impeller with a volute are also very similar. The data refer to operation in water at room temperature, flow coefficient $\phi = 0.092$, rotational speed $\Omega = 1000$ rpm, and variable whirl speed.

The calculated rotordynamic forces shown in the figures have been nondimensionalized by $\pi\varepsilon\rho_L r_T^2 \Omega^2 b$. Comparison with the experimental results by Jery, 1987 [12] (Fig. 6) shows that the calculated forces are about six times smaller than experimentally measured, but their familiar quadratic behavior with the whirl speed is well captured by the theoretical results and the vertex of the parabola is correctly located. The reasons for the observed discrepancy have not been identified with certainty, but they are likely to be mostly related to the approximate nature of the boundary conditions at the inlet and outlet sections of the impeller. In their present form these boundary conditions do not realistically account for the dynamic response of the flow in the impeller eye and diffuser (or volute). The inclusion of these effects would introduce significant additional contributions to the inertial reaction of the flow on the impeller, increasing the magnitude of the rotordynamic forces.

Clearly with present notations rotordynamic forces are destabilizing when the radial component is positive and, for the onset of nonsynchronous whirl, when the tangential component has the same sign as the whirl speed ω. Hence, with reference to Figure 6, the predicted radial force is generally destabilizing except near synchronous conditions ($\omega \cong \Omega$), while the tangential force would promote subsynchronous shaft motions in the range of whirl speeds $0 < \omega < 0.7$. Also notice that both components of the rotordynamic force are relatively small in the vicinity of $\omega/\Omega = 0.5$, corresponding to the familiar "whip conditions" of journal bearings (Newkirk and Taylor, 1925 [32], Hori, 1959 [33]).

Present results for radial turbopumps are also radically different from those obtained for cavitating inducers. In this case both the experiments of Bhattacharyya et al., 1997 [34], and our previous theoretical investigations based on the same approach used herein (d'Agostino, d'Auria and Brennen, 1998 [28]; d'Agostino and Venturini, 2002 [9]) showed a more complex dependence of the rotordynamic forces on the whirl speed. The spectral response of these forces as functions of the whirl frequency displayed a number of multiple peaks, which the theory indicated to be related with the occurrence of internal resonances of the cavitating flow in the blade channels under the excitation provided by the eccentric motion of the inducer. From the mathematical standpoint, these resonances are the consequence of the (nearly) real nature of the flow eigenvalues, which leads to an infinite set of lowly-damped critical whirl speeds, symmetrically located above and below the rotational speed Ω (synchronous conditions). Physically, the peaks of the rotordynamic forces are due to the occurrence of standing pressure waves with frequency-dependent wavelength in the blade channels. Hence, at some specific excitation frequencies the wavelength of the resonant flow perturbations is commensurable with the revolution of the blade channel around the hub. In this case the pressure distribution acts in a strong and spatially coherent fashion on the inducer, leading to the intensification of the resulting forces.

Rotordynamic forces on radial impellers, on the other hand, do not peak at any whirl frequency. Mathematically, in this case the critical whirl speeds are (nearly) imaginary:

$$\omega'_m = \pm i\pi e^{-\frac{2\pi}{N_B}\sin\beta\cos\beta} \sqrt{\frac{2m}{K_E N_B r_H r_T \ln(r_T/r_H)} \tan\frac{2m\pi^2\cos^2\beta}{N_B \ln(r_T/r_H)}}$$

Physically, in radial impellers the presence of the blades prevents the formation of synchronous pressure waves with significant extension in the azimuthal direction, capable of reacting in a coherent fashion on the impeller.

Notice that the flow solution depends on the parameter K_E, whose relationship with the extent of cavitation has already been investigated in our earlier work (d'Agostino and Venturini, 2002 [9]) with the help of a quasi-homogeneous isenthalpic cavitation model with thermal effects (Rapposelli and d'Agostino, 2001 [35]). However, as mentioned earlier, rotordynamic forces are only weakly dependent on the extent of cavitation and the value of K_E.

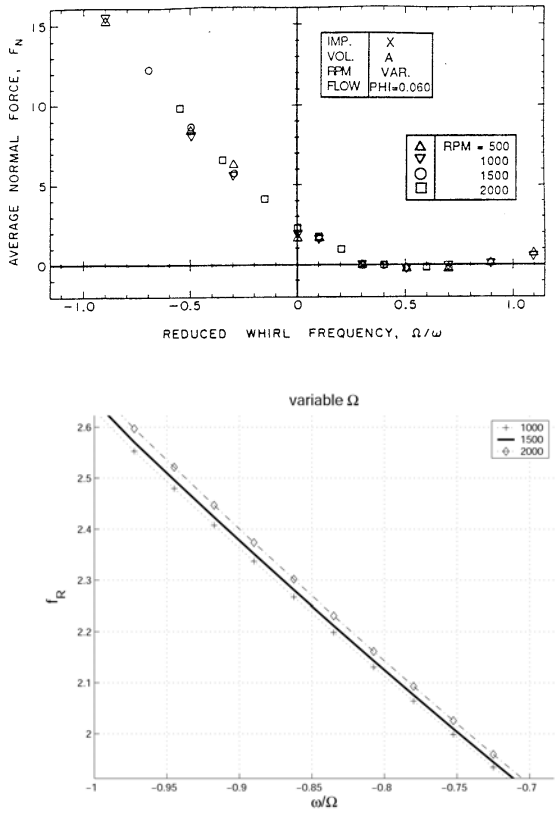

Figure 7. Comparison of the normalized radial rotordynamic force, f_R, obtained from the present theory (lower figure) for $K_E = 2 \cdot 10^{-5}$ sec^2 and several rotational speeds Ω with the experimental results (upper figure) of Jery, 1987 [12], for a centrifugal impeller with $N_B = 5$, $\phi = 0.060$, $\beta = 23°$, $r_T = 81$ mm, $b = 16$ mm and $r_H/r_T = 0.5$.

The capability of the model of qualitatively capturing the main phenomena controlling the development of rotordynamic

fluid forces in whirling centrifugal impellers is confirmed by Figures 7 and 8, which illustrate the sensitivity of the solution to changes of the rotational speed Ω and flow coefficient ϕ. In both cases the predicted impact of these parameters is small, consistently with typical experimental results from Jery, 1987 [12], shown in the upper parts of the figures. The forces in Figure 7 have been calculated with fixed K_E and therefore variable $E = \Omega^2 K_E$. With variable Ω and constant E the computed curves overlap, showing that E is a well-suited similarity parameter for cavitation effects. Besides, the curves computed for constant Ω and variable E (not shown here) almost overlap, confirming that in radial impellers the rotordynamic forces are practically insensitive to cavitation, in accordance with the experimental data by Franz et al. 1989 [29].

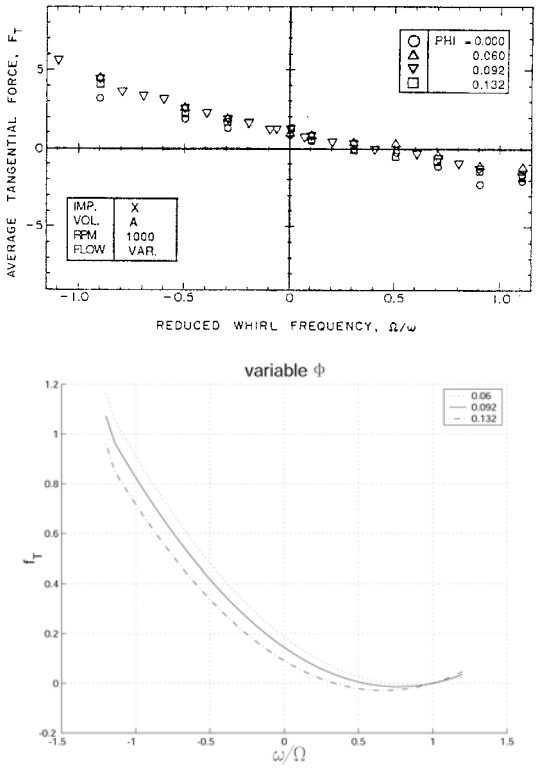

Figure 8. Comparison of the normalized tangential rotordynamic force, f_T, obtained from the present theory (lower figure) for $\Omega^2 K_E = 2$ and several rotational speeds Ω with the experimental results (upper figure) of Jery, 1987 [12], for a centrifugal impeller with $N_B = 5$, $\phi = 0.060$, $\beta = 23°$, $r_T = 81$ mm, $b = 16$ mm and $r_H / r_T = 0.5$.

Figure 8 shows the negligible influence of the flow coefficient ϕ on the rotordynamic forces: that again agrees with the experimental data. However, it should be emphasized that different values of Ω and ϕ correspond to very different rotordynamic forces in axial inducers, and that our approach to cavitation modeling correctly reflect this aspect (d'Agostino and Venturini, 2002 [9]; Venturini, 2003 [36]).

The present theory can also be used to investigate the dependence of rotordynamic whirl forces on the impeller geometry. Specifically, Figures 9, 10 and 11 illustrate the predicted effects of the number of blades, N_B, the blade angle, β, and the hub-to-tip radius ratio, r_H / r_T. As expected, the magnitude of rotordynamic forces decreases as the number of blades increases, but their stabilizing/destabilizing nature is not significantly affected (Figure 9). In this respect it is worth noting that the accuracy of the model increases with N_B because the spiral coordinate system more closely approximates the actual geometry of the impeller when the blade channels are narrower.

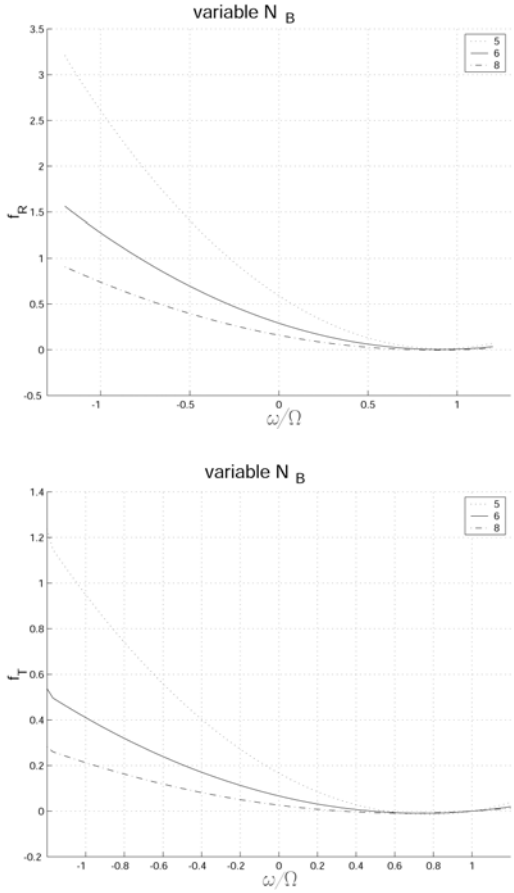

Figure 9. Normalized radial (upper figure) and tangential (lower figure) rotordynamic forces, f_R and f_T, predicted by the present theory as functions of the whirl ratio ω/Ω for a centrifugal impeller with variable number of blades $N_B = 5$ (dotted line), 6 (solid line) and 8 (dash-dotted line), $\Omega = 1000$ rpm, $\phi = 0.092$, $\beta = 23°$, $r_T = 81$ mm, $r_H = 40$ mm, $b = 16$ mm and $\Omega^2 K_E = 1$.

Figure 10 shows that both the radial and tangential components of the rotordynamic force decrease at lower blade angles. At higher values of $\beta = 40°$ the radial force is destabilizing only for negative whirl, and the tangential force undergoes two zero crossings, being potentially destabilizing only for supersynchronous whirl ($\omega/\Omega > 1$), where, however, the radial force is not capable of sustaining the eccentricity of the impeller.

Finally, Figure 11 shows that rotordynamic forces and their stabilizing/destabilizing properties are relatively insensitive to the hub-to-tip radius ratio, at least in the range of values meaningful for radial impellers.

CONCLUSIONS

The present theory predicts that blade cavitation does not appreciably modify rotordynamic fluid forces on whirling and centrifugal impellers, in accordance with the experimental evidence and in striking contrast with the observed behavior of axial inducers.

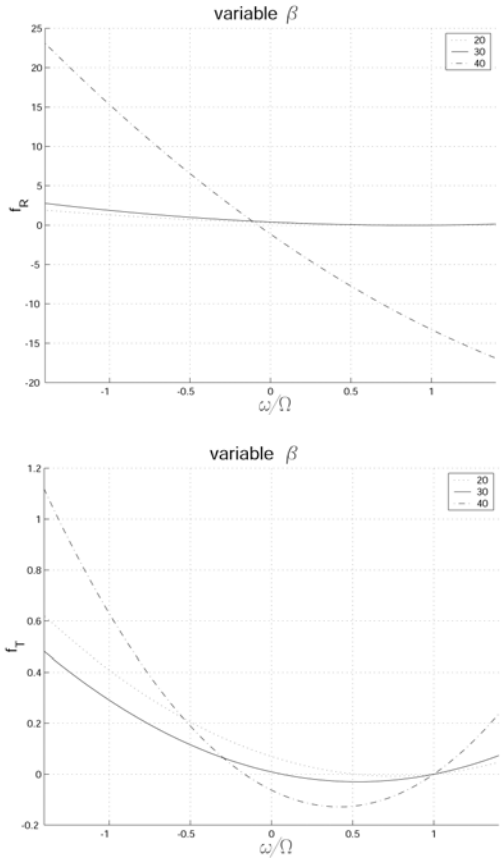

Figure 10. Normalized radial (upper figure) and tangential (lower figure) rotordynamic forces, f_R and f_T, predicted by the present theory as functions of the whirl ratio ω/Ω for a centrifugal impeller with variable blade angle $\beta = 20°$ (dotted line), 30° (solid line) and 40° (dash-dotted line), $N_B = 7$, $\Omega = 1000$ rpm, $\phi = 0.092$, $r_T = 81$ mm, $r_H = 40$ mm, $b = 16$ mm and $\Omega^2 K_E = 1$.

Comparison with the results of a similar analysis of cavitating inducers confirms that the contribution of cavitation to the rotordynamic whirl forces is only significant when the standing pressure waves excited in the blade channels by the impeller motion are capable of exerting a synchronous and coherent action on the rotor. For this to happen:

- the blade channels must be long enough in the azimuthal direction for the pressure wave to become at least partly coherent with the channel rotation around the axis: only in this case the resulting forces do not average out and generate appreciable fluid reactions on the rotor;
- possibly the cavitating flow in the blade channels must become resonant, in order to maximize the amplitude of the pressure fluctuations.

The first condition can never be satisfied in radial impellers due to the limited azimuthal extension of the blade channels. This geometric limitation is the essential reason for the different behavior rotordynamic whirl forces in cavitating radial and axial impellers. According to the predictions of the present theory, not even the second condition is verified, since natural frequencies are essentially imaginary.

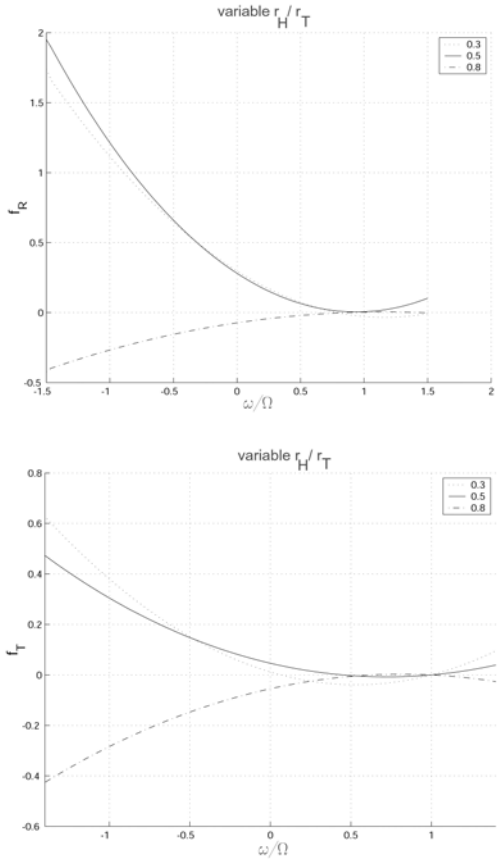

Figure 11. Normalized radial (upper figure) and tangential (lower figure) rotordynamic forces, f_R and f_T, predicted by the present theory as functions of the whirl ratio ω/Ω for a centrifugal impeller with variable hub-to-tip radius ratio $r_H/r_T = 0.3$ (dotted line), 0.5 (solid line) and 0.8 (dash-dotted line), $N_B = 7$, $\Omega = 1000$ rpm, $\phi = 0.092$, $\beta = 23°$, $r_T = 81$ mm, $b = 16$ mm and $\Omega^2 K_E = 1$.

ACKNOWLEDGEMENTS

The present work has been supported by the Agenzia Spaziale Italiana under the 2001 contract for fundamental research. The authors would like to express their gratitude to Profs. Mariano Andrenucci and Renzo Lazzeretti of the Dipartimento di Ingegneria Aerospaziale, Università di Pisa, Pisa, Italy, for their constant and friendly encouragement.

REFERENCES

[1] Thomas J.H., 1958, "Instabile Eigenschwingungen von Turbinenlaufern Angefacht durch die Spaltstroemung in Stopfubuchsen und Bechauchflug (Unstable Natural Vibrations of Turbine Rotors

Induced by Clearance Flows in Glands and Bladings)", *Bull. De. L.A.I.M.,* **71**, 1039-1063.

[2] Alford J.S., 1958, "Protecting Turbomachinery from Self-Excited Rotor Whirl", *ASME J. Eng. Power*, **87**, 333-334.

[3] Martinez-Sanchez M., Jaroux B., Song S.J. and Yoo S., 1995, "Measurement of Turbine Blade-Tip Rotordynamic Excitation Forces", *ASME J. Turbomachinery*, **117**, 384-393.

[4] Martinez-Sanchez M. and Song S.J., 1997a, "Rotordynamic Forces Due to Turbine Tip Leakage-Part I: Blade Scale Effects", *ASME J. Turbomachinery*, **119**, 695-703.

[5] Martinez-Sanchez M. and Song S.J., 1997b, "Rotordynamic Forces Due to Turbine Tip Leakage-Part II: Radius Scale Effects and Experimental Verification", *ASME J. Turbomachinery*, **119**, 704-717.

[6] d'Auria, F., d'Agostino, L., Brennen, C.E., 1995, "Bubble Dynamics Effects on the Rotordynamics Forces in Cavitating Inducers", *ASME-FED* **201**, 47-54.

[7] d'Agostino L. and d'Auria F., 1997, "Three-Dimensional Analysis of Rotordynamic Forces on Whirling and Cavitating Inducers", *ASME Paper FEDSM97-3335*.

[8] d'Agostino L., d'Auria F. and Brennen C.E., 1998, "A Three-Dimensional Analysis of Rotordynamic Forces on Whirling and Cavitating Helical Inducers", *ASME J. Fluids Eng.*, **120**, 698-704.

[9] d'Agostino L. and Venturini-Autieri M.R., 2002, "Three-Dimensional Analysis of Rotordynamic Fluid Forces on Whirling and Cavitating Finite-Length Inducers", *9th Int. Symp. on Transport Phenomena and Dynamics of Rotating Machinery (ISROMAC-9)*, Honolulu, HI, USA, February 10-14.

[10] Chamieh D.S. et al., 1985, "Experimental Measurements of Hydrodynamic Radial Forces and Stiffness Matrices for a Centrifugal Pump Impeller", *ASME J. Fluids Eng.*, **107**, 307-315.

[11] Jery B., Acosta A. J., and Caughey T. K., 1985, "Forces on Centrifugal Pump Impellers", *Proc. 2nd Int. Pump Symp.,* Houston, TX, USA, April 29-May 2.

[12] Jery B., 1987, "Experimental Study of Unsteady Hydrodynamic Force Matrices on Whirling Centrifugal Pump Impellers", *Report No. E200.22*, Div. Eng. & Applied Sciences, California Institute of Technology, Pasadena, CA, USA.

[13] Shoji, H. and Ohashi, H., 1987, "Lateral Fluid Forces on Whirling Centrifugal Impeller (1st Report: Theory)", *ASME J. Fluids Eng.*, **109**, 94-99.

[14] Ohasi H. and Shoji H., 1987, "Lateral Fluid Forces on Whirling Centrifugal Impeller (2nd Report: Experiment in Vaneless Diffuser)", *ASME J. Fluids Eng.*, **109**, 100-106.

[15] Adkins, D.R. and Brennen, C.E., 1988, "Analysis of Hydrodynamic Radial Forces on Centrifugal Pump Impeller", *ASME J. Fluids Eng.*, **110**, 20-28.

[16] Arndt N. et al., 1989, "Rotor-Stator Interaction in a Diffuser Pump", *ASME J. Turbomachinery*, **111**, 213-221.

[17] Arndt N. et al., 1990, "Experimental Investigation of Rotor-Stator Interaction in a Centrifugal Pump with Several Vaned Diffusers", *ASME J. Turbomachinery*, **112**, 98-108.

[18] Tsujimoto, Y, Yoshida, Y., Ohashi, H., Teramoto, N. and Ishizaki, S., 1997, "Fluid Force Moment on a Centrifugal Impeller Shroud in Precessing Motion", *ASME J. Fluids Eng.*, **119**, 366-371.

[19] Uy, R.V., and Brennen, C.E., 1999, "Experimental Measurements of Rotordynamic Forces Caused by Front Shroud Pump Leakage", *ASME J. Fluids Eng.*, **121**, 633-637.

[20] Baskharone, E.A., 1999, "Swirl Brake Effect on the Rotordynamic Stability of a Shrouded Impeller", *ASME J. Turbomachinery*, **121**, 127-133.

[21] Hiwata A. and Tsujimoto Y., 2002, "Theoretical Analysis of Fluid Forces on and Open-Type Centrifugal Impeller in Whirling Motion", *ASME J. Fluids Eng.*, **124**, 342-347.

[22] Rosenmann, W., 1965, "Experimental Investigations of Hydrodynamically Induced Shaft Forces with a Three Bladed Inducer", *Proc. ASME Symp. on Cavitation in Fluid Machinery*, 172-195.

[23] Arndt, N., and Franz, R., 1986, "Observation of Hydrodynamic Forces on Several Inducers Including the SSME LPOTP", *Report No. E249.3*, Div. Eng. and Applied Sciences, California Institute of Technology, Pasadena, CA, USA.

[24] Brennen, C. E., 1994, "Hydrodynamics of Pumps", *Oxford University Press, Oxford*, England.

[25] Bhattacharyya, A., 1994, "Internal Flows and Force Matrices in Axial Flow Inducers", *Ph.D. Thesis*, Div. Eng. and Applied Science, California Institute of Technology, Pasadena, CA, USA.

[26] d'Auria, F., d'Agostino, L., Brennen, C.E., 1995, "Bubble Dynamics Effects on the Rotordynamics Forces in Cavitating Inducers", *ASME-FED* **201**, 47-54.

[27] d'Agostino L. and d'Auria F., 1997, "Three-Dimensional Analysis of Rotordynamic Forces on Whirling and Cavitating Inducers", *ASME Paper FEDSM97-3335*.

[28] d'Agostino L., d'Auria F. and Brennen C.E., 1998, "A Three-Dimensional Analysis of Rotordynamic Forces on Whirling and Cavitating Helical Inducers", *ASME J. Fluids Eng.*, **120**, 698-704.

[29] Franz R. et al., 1989, "The Rotordynamic Forces on a Centrifugal Pump Impeller in the Presence of Cavitation", *ASME-F.E.D.* **81**, 205-212.

[30] Campos L.M.B.C. and Gil P.J.S., 1995, "On Spiral Coordinates with Application to Wave Propagation", *J. Fluid Mechanics*, **301**, 153-173.

[31] Visser F.C., 1999, "On the Asymptotic Solution of the Poisson Equation Describing the Two-Dimensional Incompressible Inviscid Flow in a Rotating Centrifugal Impeller", *Zeitschrift für Angewandte Mathematik und Mechanik*, **79** (5), 353-356.

[32] Newkirk B.L. and Taylor H.D., 1925, "Shaft Whipping due to Oil Action in Journal Bearing", *General Electric Review*, August 1925, 559-568.

[33] Hori Y., 1959, "The Theory of Oil Whip", *ASME J. Appl. Mech*., **26**, 189-198.

[34] Bhattacharyya, A., Acosta, A.J., Brennen, C.E., and Caughey, T.K., 1997, "Rotordynamic Forces in Cavitating Inducers", *ASME J. Fluids Eng.*, **199**, No. 4, 768-774.

[35] Rapposelli, E., and d'Agostino, L., 2001, "A Modified Isenthalpic Model of Cavitation in Plane Journal Bearings", *CAV2001, Int. Symp. on Cavitation*, Pasadena, CA, USA, June 20-23.

[36] Venturini-Autieri M.R., 2003, "Analisi delle Forze Rotodinamiche in Turbomacchine Cavitanti", *Tesi di Laurea*, Dipartimento di Ingegneria Aerospaziale, Università di Pisa, Pisa, Italy.